JOURNAL OF COMPUTATIONAL PHYSICS 19, 1–28 (1975)

A Geometrical Approach to Calculating the Energy and Frequency Spectra of Crystals*

T. POSTON AND A. B. BUDGOR

Institute for Fundamental Studies, Departments of Mathematics and Physics, University of Rochester, Rochester, New York 14627

Received January 15, 1975; revised March 10, 1975

A new histogram approach for calculating the electronic or vibrational spectra of crystals is introduced which does not require the elaborate root-searching procedures of Gilat and his co-workers. The spectra are obtained by numerically computing the area between curves of constant x, x denoting either the frequency variable ν^2, or energy variable E, which are found from a dispersion relation $f(\phi, x) = 0$, ϕ being the wave vector in the first Brillouin zone. This relation defines a hypersurface S of possible states in the space of possible pairs (ϕ, x) of wave vectors and values of x. The technique is no less accurate at points where the surface becomes flat, i.e., at maxima, minima, and saddles and yields quite accurate representations of the van Hove singularities. Around any particular value of x the spacing and, if desirable, the number of points on the contours can be refined without increasing the computational time by finer calculations where they are clearly unnecessary. Since no root searching in x is required, this method is completely general and is not highly constrained by crystal symmetry types. Thus, very complicated dispersion relations in x can be handled. The technique is illustrated by computing the spectra of a 2-D vibrational and electronic system. Results for several 3-D vibrational and electronic systems have been obtained and are in good agreement with previous analytic calculations where these exist.

I. PROBLEM AND TECHNIQUES

Two basic equations which characterize many phenomena in continuous media are the wave equation,

$$\frac{\partial^2 f}{\partial t^2} = c^2 \nabla^2 f, \tag{1}$$

which describes a wave propagating with velocity c in the medium, and the diffusion (or heat conduction) equation,

$$\frac{\partial f}{\partial t} = D \nabla^2 f, \tag{2}$$

which appears for processes involving dissipation.

* Work partially supported by Grant No. GU-4040 of the National Science Foundation.

In the transition from the continuum to a discrete medium similar equations arise, but they involve second differences rather than ∇^2. The subsequent discussion will concentrate on two network models of crystalline solids inspired by the ball and wire models constructed by crystallographers. Thus, if we wish to discuss the vibrations of crystal lattices the wires connecting the balls representing atoms are replaced by springs and Eq. (1) is replaced by its analogous differential-difference equation. There is a similar substitution for Eq. (2) when we wish to consider the dynamics or kinematics of electrons on a lattice. Here we assume that the electrons are restricted to move only along the wires, or bonds, connecting atoms.

The determination of the vibrational and electronic properties of these model crystals has been exhaustively discussed by Maradudin *et al.* and by Montroll and his co-workers, respectively, with the unifying characteristic that the allowed vibrational and electronic band structures are derivable from the determinantal solution of the dynamical or connectivity matrix, M_{vib} and M_{el} [1, 2, 3].

To determine the vibronic and thermodynamic functions for a crystal one must know how the frequencies of lattice vibrations and the electronic energy states are distributed in frequency and energy space, respectively. In the case of a finite crystal with N atoms and periodic boundary conditions, this means knowing how many of the finite set of possible wave vectors ϕ in the first Brillouin zone have

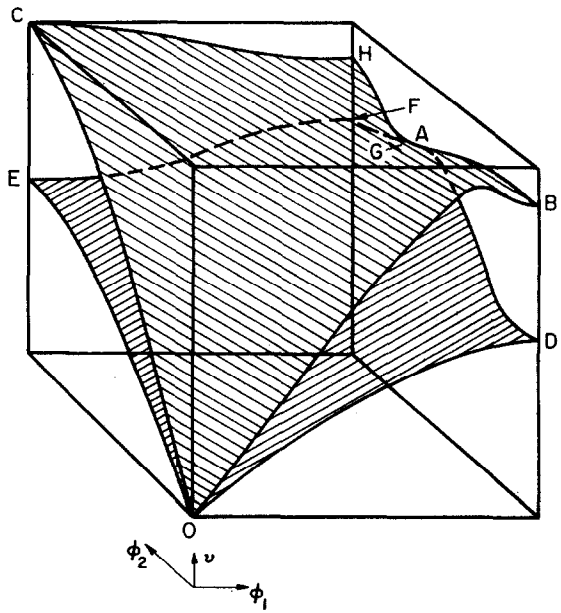

FIG. 1a. The hypersurface S of possible vibrational states in the case of a 2-D square lattice having nearest- and next-nearest neighbor interactions.

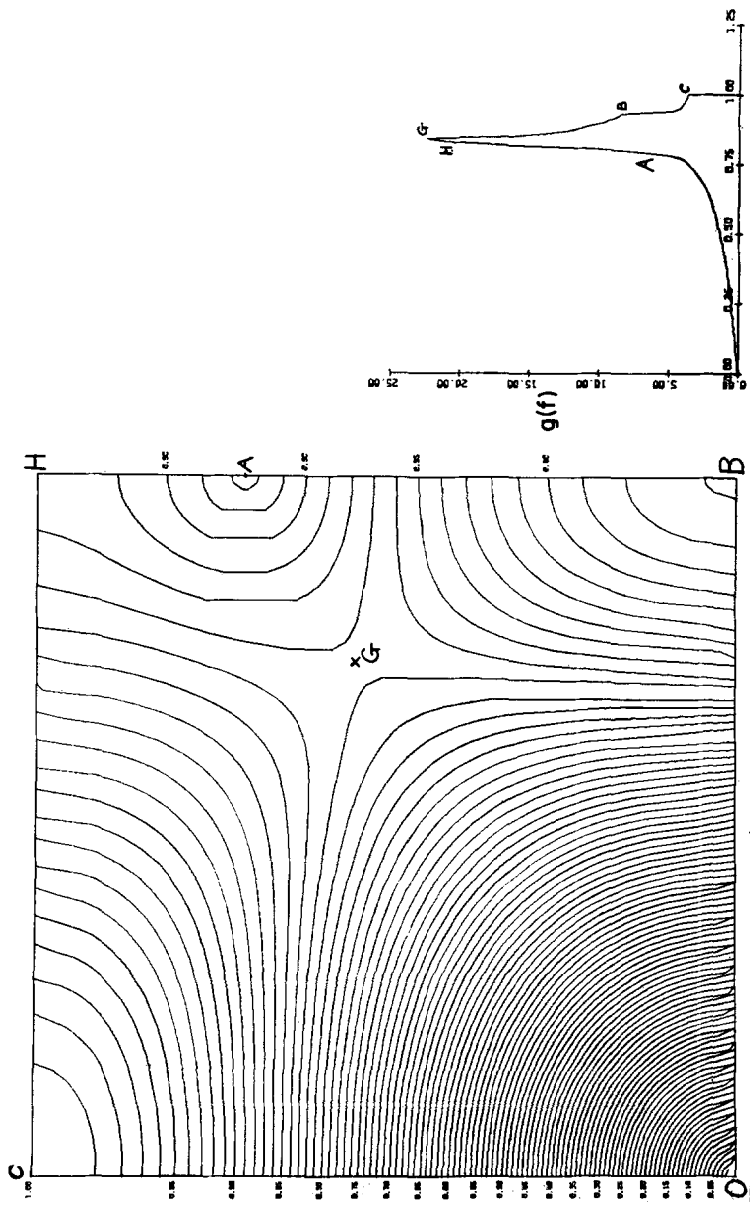

FIG. 1b. *Contour map and frequency spectrum for the + branch of the aforementioned 2-D square lattice when* $\epsilon = 0.8$ *and* $\tau = \frac{1}{3}$. *The numbers at the sides of the square identify the value of* $f = \nu/\nu_L$ *for each contour.*

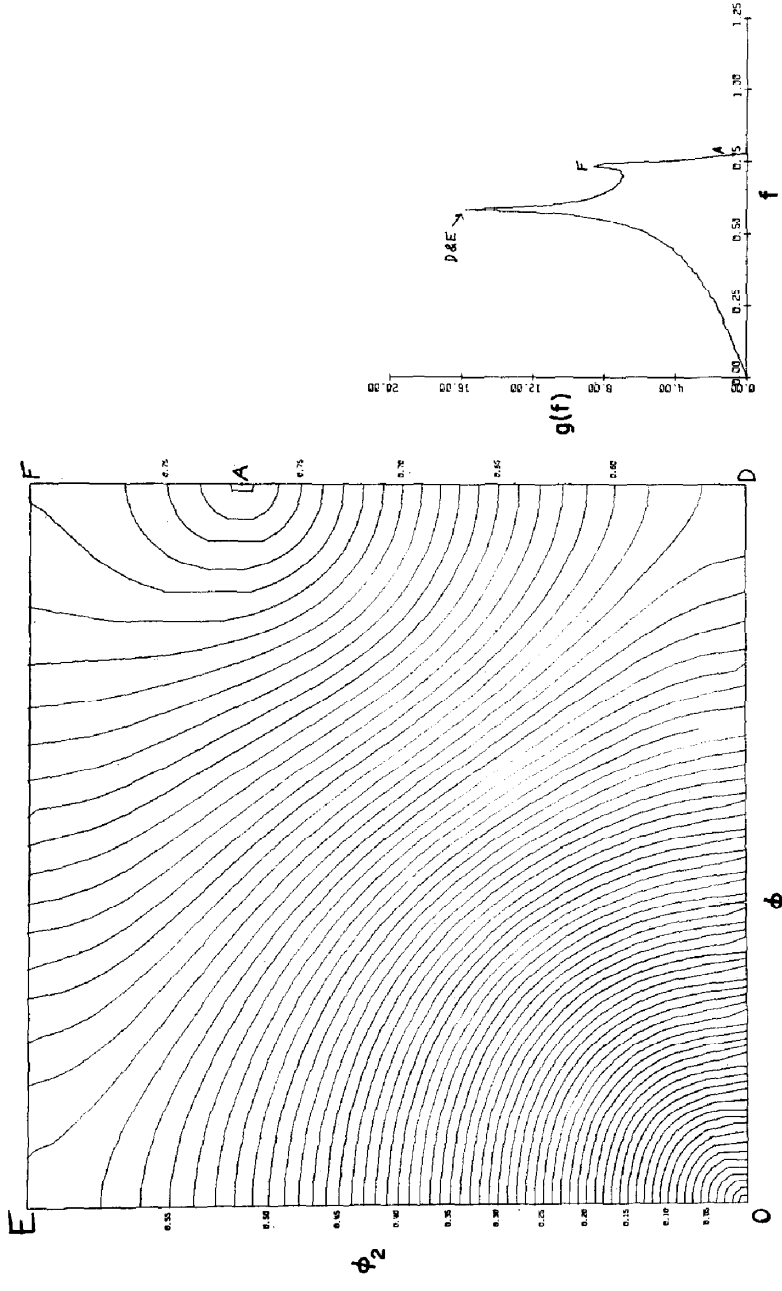

FIG. 1c. — branch, $\epsilon = 0.8$, and $\tau = \frac{1}{8}$.

states lying between x and $x + \Delta x$ (x denoting either the frequency variable, ν^2, or energy variable E). In the limit as N goes to infinity, we have an equation (the *dispersion relation*) of the form $f(\phi, x) = 0$, defining a hypersurface S of possible states in the space of possible pairs (ϕ, x) of wave vectors and values of x. The number of vectors having states between x and $x + \Delta x$ must now be replaced by a measure, this being ordinary area in the space of vectors in the first Brillouin zone, or other convenient period in ϕ-space. Taking the limit as $\Delta x \to 0$ gives the "density of states function" or spectrum $g(x)$ at x.

In vibrational problems the dispersion relation $\det(M_{\text{vib}}) = 0$ gives an eigenvalue problem in ν^2, and since M_{vib} is self-adjoint the hypersurface S can be considered as a multibranched function of ϕ. This is illustrated in Fig. 1a in the case of a 2-D square lattice having nearest- and next-nearest neighbor interactions, with ϕ lying in $[0, \pi] \times [0, \pi]$; the rest of the surface is given by reflection in the $\phi_1 - \nu^2$ and $\phi_2 - \nu^2$ planes and translation by $2n\pi$ in the ϕ_1 and ϕ_2 directions. (Such an explicit separation into branches is fundamental to the exact solution techniques for g in use and severely restricts the rank of M_{vib} if such analysis is to be possible.) Figures 1b and 1c show the corresponding contour maps and spectra. Spectrum singularities arise from points at which the surface considered is parallel to the ϕ-plane, generally maxima, minima, and saddles. Non-Morse-type singularities can occur when stabilized by the symmetries of the problem. (See van Hove [4] and Montroll [5] for a discussion of the relevant applications of Morse theory and the classification of the corresponding singularities in g.) The distinction between the branches has physical significance and makes the separate computation of the branch spectra, as illustrated, useful.

In electronic problems E enters M_{el} nonlinearly, and is not restricted to the diagonal. Geometrically, then, S cannot with any naturalness be considered as a branched function. Figures 2a and 2b show a contour map and perspective drawing for a typical case.

From 1912, when Born and von Karman [6] first derived an expression for the frequency distribution of one-dimensional lattice vibrations, much effort has gone into determining g for a variety of crystal symmetries. Several exact 2-D and 3-D calculations have been performed for crystals with special symmetries. However, their difficulty increases rapidly with realism of the model. For example, while the determination of $g(\nu^2)$ for a 2-D square lattice with anisotropic nearest-neighbor interactions is comparatively straightforward [5], with the introduction of next-nearest-neighbor forces [7] even the case with isotropic nearest neighbors requires $\tau = 1/[1 + (2\alpha/\gamma)] = \frac{1}{3}$ for an exact solution to be possible (α and γ are nearest- and next-nearest-neighbor force constants, respectively). Only qualitative results are given for $\tau \neq \frac{1}{3}$, and anisotropy in nearest neighbors is not considered. Thus in most realistic cases, numerical techniques must be used.

Due to the recent nature of the electrons on a network model the only approxi-

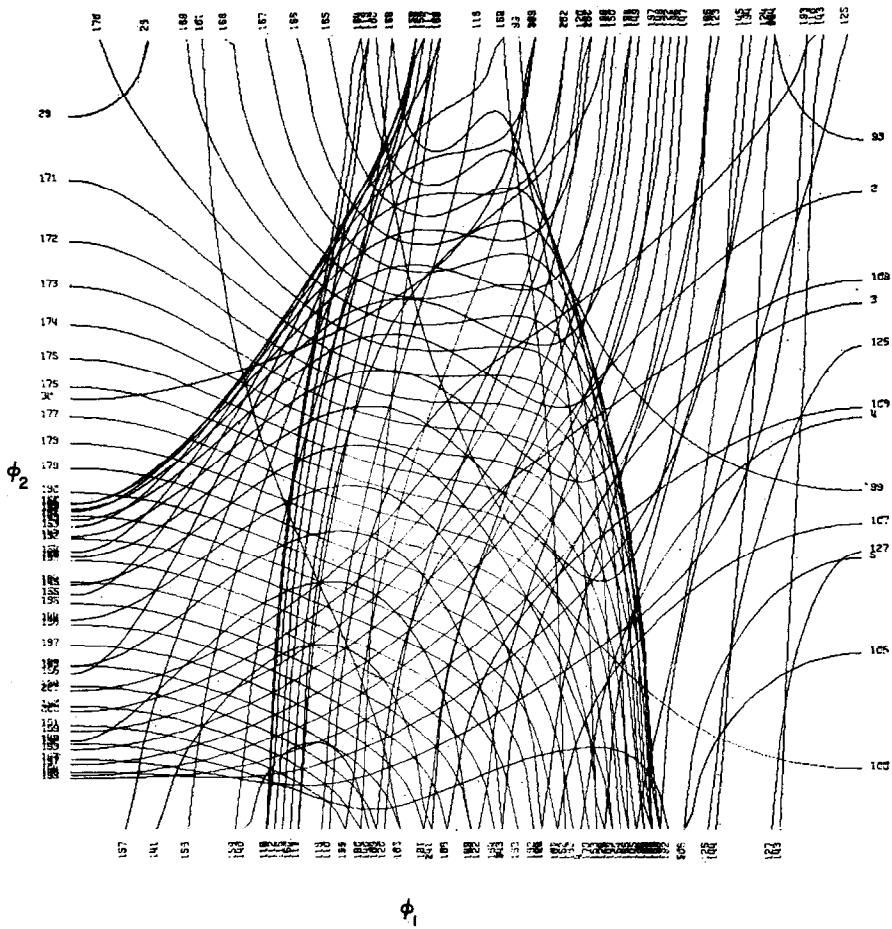

FIG. 2a. Typical contour map derived from an electronic dispersion relation which is a sixth-order polynomial equation in an awkward function of E, with coefficients depending on ϕ. The numbers at the sides of the square identify the value of E for each contour.

mate spectrum calculations that have been performed are for lattice vibrations, of which the most accurate and conceptually the simplest is the root sampling method. Here the secular equation is solved at a large number of uniformly distributed points in the first Brillouin zone and the spectrum approximated by a normalized histogram.

The disadvantages of this technique are:

(i) For accuracy, a very large number of points are required.

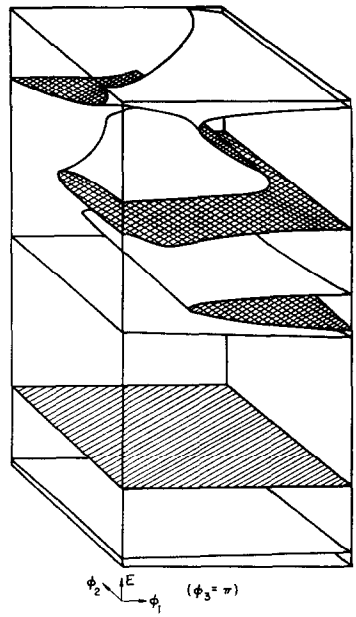

FIG. 2b. Perspective drawing of the surface whose contour map is Fig. 2a.

(ii) The technique is least accurate at the most important values of ν^2, the singularities of g.

(iii) Improvement of accuracy at any one frequency level requires the same refinement everywhere.

(iv) Each crystal symmetry type essentially requires the development of a new, highly complex program. The best of these are due to Gilat and his co-workers [8, 9] and use a linear approximation around each value of $\boldsymbol{\phi}$. This reduces the amount of root-searching, and cost, but greatly elaborates the program. Moreover it requires the gradient vector of each ν_i^2 at $\boldsymbol{\phi}$, which often is not easily obtainable in analytic form and thus may necessitate a risky numerical differentiation.

Our technique is suggested by the method of studying singularities developed in Woodcock and Poston [10], with a similar method developed by Faulkner *et al.* [22]. We describe it first for a 2-D lattice. Instead of calculating x for given $\boldsymbol{\phi}$, we fix successive values of x and compute one component of $\boldsymbol{\phi}$ in terms of the other. This yields the fixed-x contours of the surface. The area between the x and $(x + \Delta x)$ contours projected to $\boldsymbol{\phi}$-space is exactly

$$\int_x^{x+\Delta x} g \, dx, \tag{3}$$

so that numerical calculation of this area gives a very good histogram value for g. Recall that in the usual technique for computing area between curves, a local linear approximation is automatic, with no gradient calculations necessary. This is illustrated in Fig. 3, where the number obtained by adding the distances

$$| y(x + \delta x, z_i) - y(x, z_i)|$$

is proportional to the sum of the areas of the illustrated parallelograms.

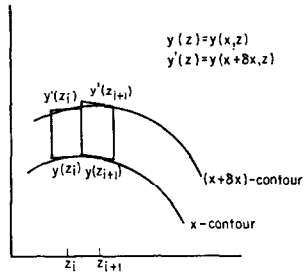

FIG. 3. Technique used to compute the area between contours.

In a 3-D problem this approach is repeated for a set of parallel slices of ϕ-space and uses a similar automatic local linear approximation with the resulting histogram values for g added. Results for several 3-D vibrational and electronic systems have been obtained and are in good agreement with previous analytic calculations where these exist. This work will be reported in [11].

An added feature of this technique is that it makes no appeal to the view of S as a branched function. In fact while lack of a neat branch structure complicates earlier approaches, it simplifies this one, since to distinguish between branches can be quite complicated and costly. The results are in no way less accurate at singularities than elsewhere (subject to the essential nature of any histogram, which must necessarily miss the full height of a "spike" singularity.) Around any energy or frequency level of special interest, the spacing and, if desirable, the number of points on the contours can be refined without increasing the computational time by finer calculations where they are clearly unnecessary. The special symmetries of a particular problem can be taken advantage of by minor alterations in programming, rather than the fundamental alterations needed in root-sampling techniques when extending applicability from the cubic crystals to crystals of other symmetries, such as hexagonal and tetragonal [23, 24]. This is due to the fact that the starting point for our spectrum calculations is the expansion of the determinant of M_{vib} or M_{el} with subsequent rearrangement of terms to obtain a polynomial in the cosine of one of the reciprocal lattice vectors. The coefficients of this polynomial are

functions of the remaining reciprocal lattice vectors and x. Changing the symmetry of the problem just means obtaining a new polynomial equation from M_{vib} or M_{el}. The subsequent procedure for calculating $g(x)$ remains the same. Thus, the method is far more easily adaptable from one problem to another.

The degree of simplicity of this approach depends on the ease with which ϕ_2, say, can be obtained from the variables ϕ_1, ϕ_3, and x in the dispersion relation to give the contours. A typical electronic network model under study gives a sixth-order polynomial equation in an awkward function of E, with coefficients depending on ϕ. Due to the noneigenvalue nature of this model, root-searching in E would require immense computations with great difficulty attaching to the differentiation needed for any local linear approximation, but the cosine of one component of ϕ may be expressible as an *explicit* function of E and the cosines of the other two. Evaluating high-order polynomials is easier than solving them.

As long as the order of the equation is lower in at least one $\cos(\phi_i)$ than in x, it is easier to find contours in ϕ_i than roots in x. Even if the equation becomes awkward enough to require root-searching in finding the contours, however, this method still does not become as cumbersome as root-sampling because the local linear approximation remains automatic and therefore neither an immensely fine mesh nor computations of the gradient of a high-order implicitly defined multi-valued function are required. Moreover, refinement around a given value of x remains easy. An entirely general program is under development whose use will vary from problem to problem only in the specification of M_{vib} or M_{el}, and in the method used for finding ϕ_j given (ϕ_j, ϕ_k, x) which may be obtained from explicit formulas, polynomial solution, or root-searching.

One final note in passing is that this technique is directly applicable to the methods now in use in computing the electron band structure of solids (cf. the tight binding and augmented plane wave methods [12]). Invariably, since the energy bands are determined from the solution of a secular equation in E, the same procedure in obtaining g for the vibrating crystal can be used.

An essential part of the development of this technique has been the use of computer plotting of the contours: however complex a surface (e.g., Fig. 2b) the corresponding contour map (Fig. 2a) suffices to describe it. This gives both a check on whether the area computation routine is correct, since the areas are visible and the singularities identifiable for comparison with the output for g, and a check on whether the spacing of x values is sufficiently fine. (If one contour is on one branch of the surface, and the next one on another, significant error is introduced unless the spacing is fine enough to bring at least one of them close to the edge of the map. Thus, at energy or frequency levels where the contours are very far apart it may be appropriate to locally refine the spacing in x.)

II. A Vibrational Example

Consider the 2-D monatomic square lattice of Fig. 4, where we have identified lattice coordinates by the double (l, m) with each parameter ranging over the integral values $-N/2$ to $N/2$, and the components of the atomic displacements from their equilibrium positions by $u_{l,m}$ and $v_{l,m}$.

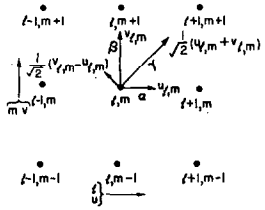

FIG 4. 2-D monatomic square lattice where α, β, and γ are the nearest- and next-nearest neighbor coupling constants.

By assuming the existence of central forces only, the total potential energy of the system can be written in terms of a quadratic form in the displacements from equilibrium,

$$V(\mathbf{r}_1, \ldots, \mathbf{r}_N) = \tfrac{1}{2} \sum_{i>j}^{N} \sum^{N} (\xi_i - \xi_j)^2 \, c(a_{ij}), \tag{4a}$$

$c(a_{ij})$ being a function of the equilibrium distance between the ith and jth atoms. If we further assume that the interatomic forces are sufficiently short-ranged that their influence is only significant up to next-nearest neighbors, but such that the nearest-neighbor coupling constants in the u and v directions are different, $V(\mathbf{r}_1, \ldots, \mathbf{r}_N)$ in terms of its components $u_{l,m}$ and $v_{l,m}$ may be rewritten as

$$\begin{aligned} V(\mathbf{r}_1, \ldots, \mathbf{r}_N) = \tfrac{1}{2} \sum_{l,m} \{ & \alpha(u_{l,m} - u_{l+1,m})^2 + \beta(v_{l,m} - v_{l,m+1})^2 \\ & + \gamma[(u_{l,m} - u_{l+1,m+1} + v_{l,m} - v_{l+1,m+1})^2 \\ & + (u_{l,m} - u_{l+1,m-1} - v_{l,m} + v_{l+1,m-1})^2]\}, \end{aligned} \tag{4b}$$

α, β, γ being the nearest- and next-nearest-neighbor coupling constants.

Application of Lagrange's equations then leads to the following equations of motion.

$$\begin{aligned} -M\ddot{u}_{l,m} = & \alpha(2u_{l,m} - u_{l+1,m} - u_{l-1,m}) \\ & + \gamma(4u_{l,m} - u_{l+1,m+1} - u_{l+1,m-1} \\ & - u_{l-1,m-1} - u_{l-1,m+1} - v_{l+1,m+1} \\ & + v_{l+1,m-1} - v_{l-1,m-1} + v_{l-1,m+1}), \end{aligned} \tag{5a}$$

and

$$-M\ddot{v}_{l,m} = \beta(2v_{l,m} - v_{l,m+1} - v_{l,m-1}) + \gamma(4v_{l,m} - v_{l+1,m+1} - v_{l-1,m+1} - v_{l-1,m-1} - v_{l+1,m-1} - u_{l+1,m+1} + u_{l-1,m+1} - u_{l-1,m-1} + u_{l+1,m-1}). \tag{5b}$$

In the limit as $N \to \infty$ one would expect that the nature of the vibrations is independent of surface effects. For convenience, then, let us impose Born–von Karman periodic boundary conditions

$$\begin{aligned} u_{l,N+1} &= u_{l,1}\,, \qquad u_{N+1,m} = u_{1,m}\,, \\ v_{l,N+1} &= v_{l,1}\,, \qquad v_{N+1,m} = v_{1,m}\,. \end{aligned} \tag{6}$$

Equations (5) may then be solved by assuming the particular periodic solutions

$$u_{l,m} = u' \exp i(2\pi\nu t + l\phi_1 + m\phi_2), \tag{7a}$$

$$v_{l,m} = v' \exp i(2\pi\nu t + l\phi_1 + m\phi_2). \tag{7b}$$

where the $\phi_j = 2\pi a_j/N$ $(j = 1, 2)$ are the phase differences for successive atoms, $N/2 \leqslant a_j \leqslant N/2$, and ν is the frequency of vibration corresponding to a particular solution. Substitution of (7) into (5) then yields,

$$-4M\pi^2\nu^2u' + 2\alpha u'(1 - \cos\phi_1) + 4\gamma u'(1 - \cos\phi_1\cos\phi_2) + 4\gamma v' \sin\phi_1 \sin\phi_2 = 0, \tag{8a}$$

$$-4M\pi^2\nu^2v' + 2\beta v'(1 - \cos\phi_2) + 4\gamma v'(1 - \cos\phi_1\cos\phi_2) + 4\gamma u' \sin\phi_1 \sin\phi_2 = 0. \tag{8b}$$

To obtain a consistent solution of these coupled equations the determinant of the coefficients of u' and v' must vanish:

$$\begin{vmatrix} A_1 - 4\pi^2\nu^2M & B \\ B & A_2 - 4\pi^2\nu^2M \end{vmatrix} = 0, \tag{9}$$

where

$$A_1 = 2\alpha(1 - \cos\phi_1) + 4\gamma(1 - \cos\phi_1\cos\phi_2), \tag{10a}$$

$$A_2 = 2\beta(1 - \cos\phi_2) + 4\gamma(1 - \cos\phi_1\cos\phi_2), \tag{10b}$$

and

$$B = 4\gamma \sin\phi_1 \sin\phi_2\,. \tag{10c}$$

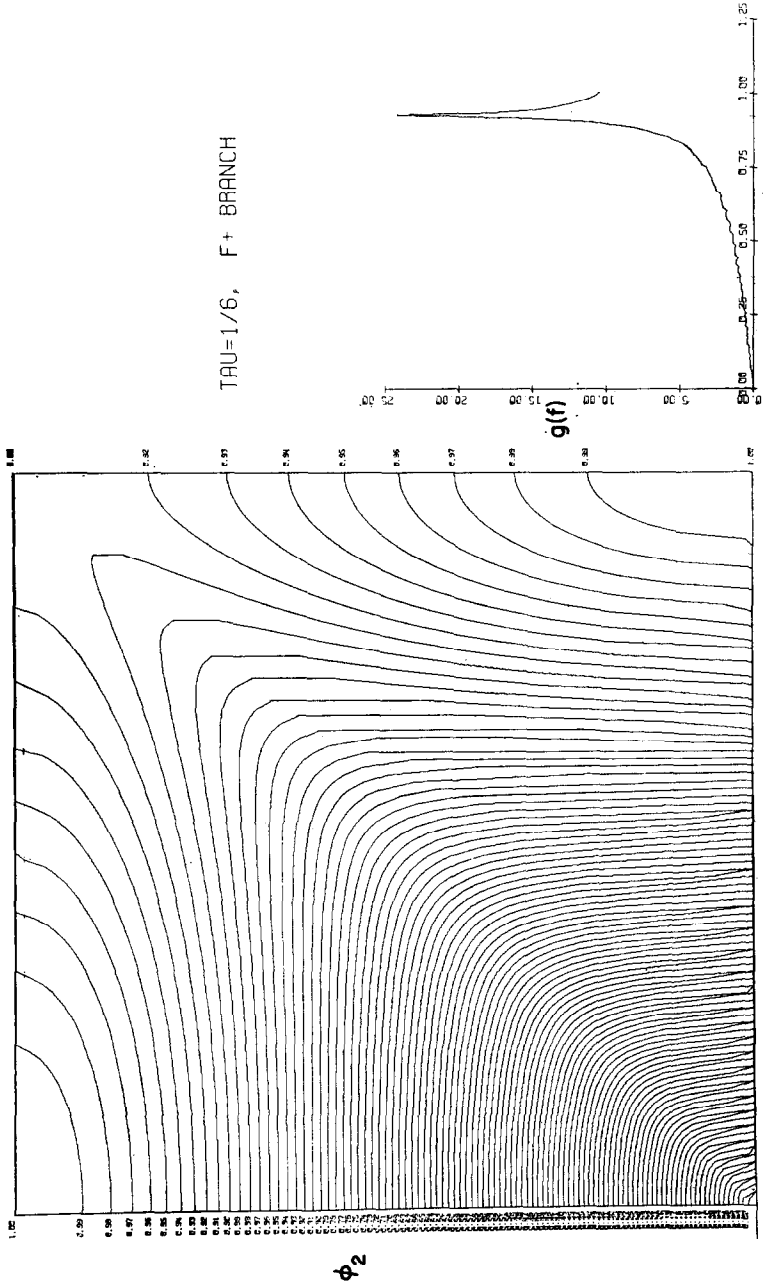

FIG. 5a. Contour maps and vibrational spectra derived from (13) for the + branch when $\epsilon = 1$ and $\tau = \frac{1}{6}$.

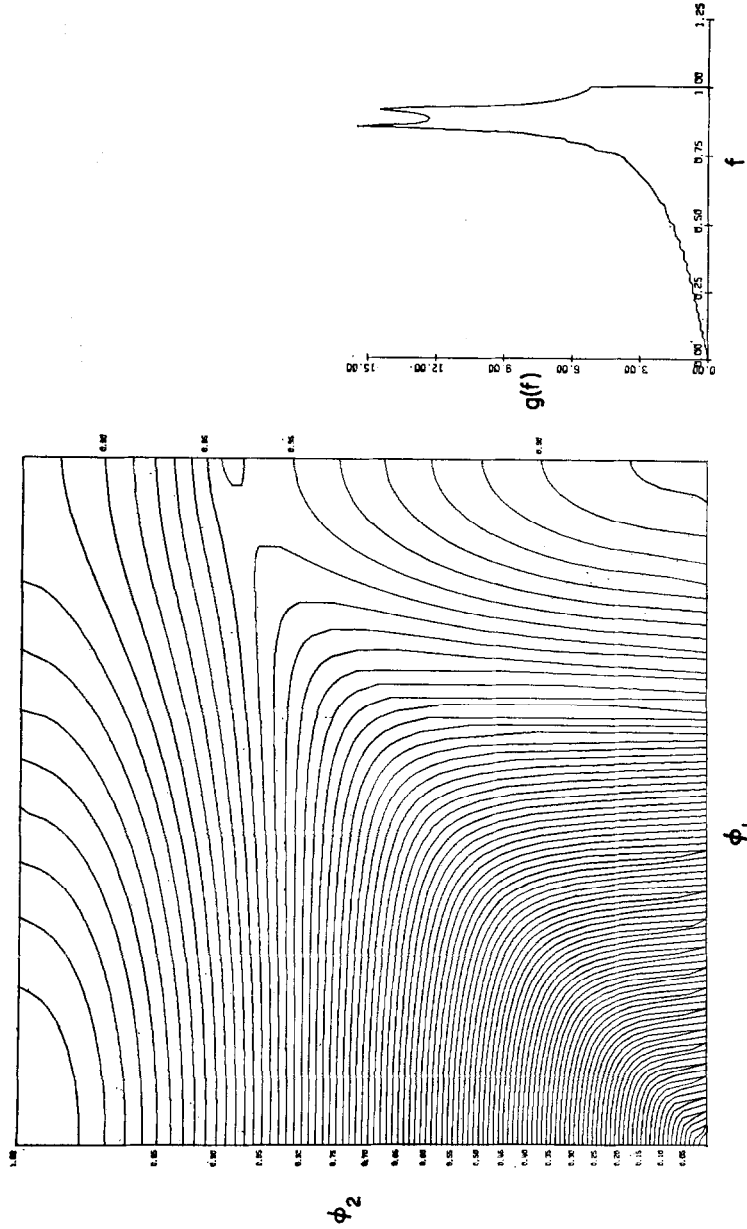

FIG. 5b. + branch, $\epsilon = 0.8$, and $\tau = \frac{1}{8}$.

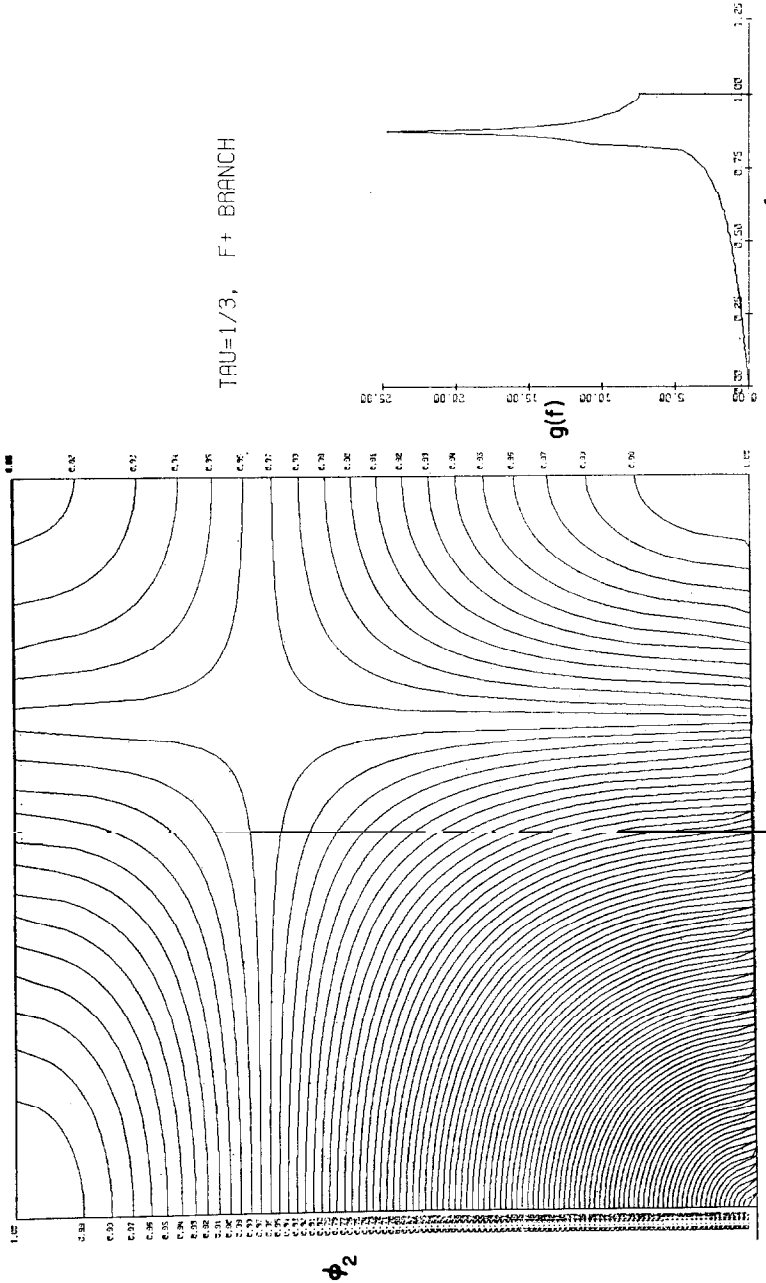

FIG. 5c. + branch, $\epsilon = 1$, and $\tau = \frac{1}{3}$.

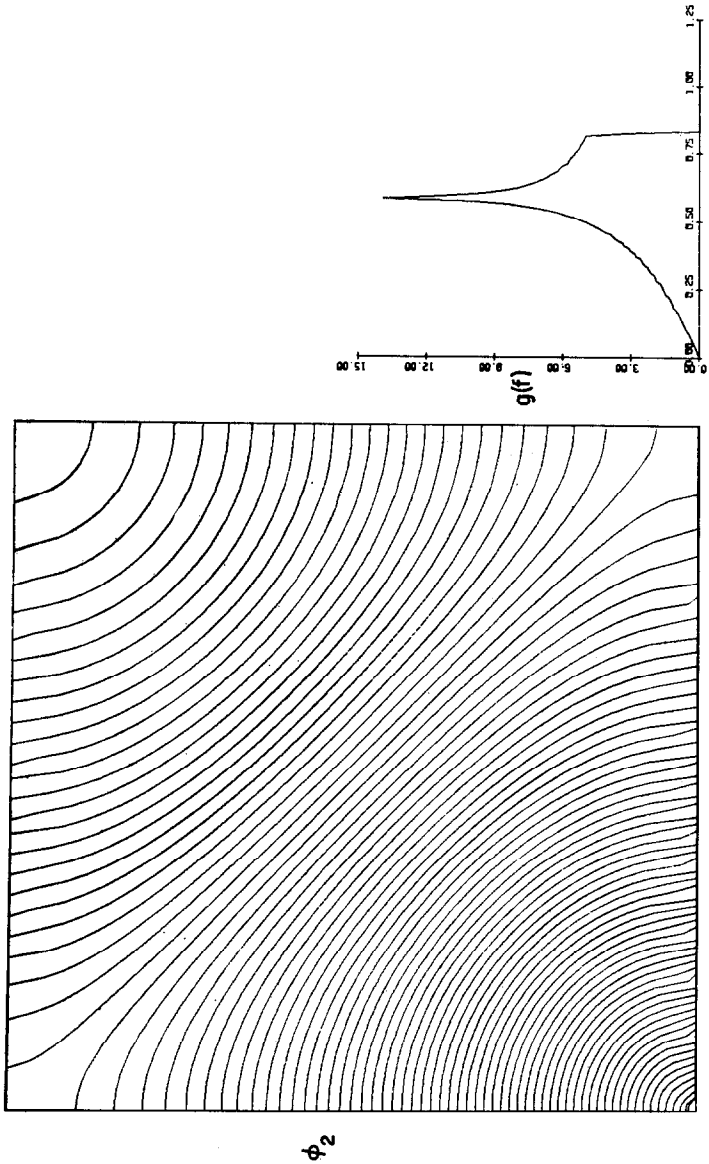

FIG. 5d. — branch, $\epsilon = 1$, and $\tau = \frac{1}{3}$.

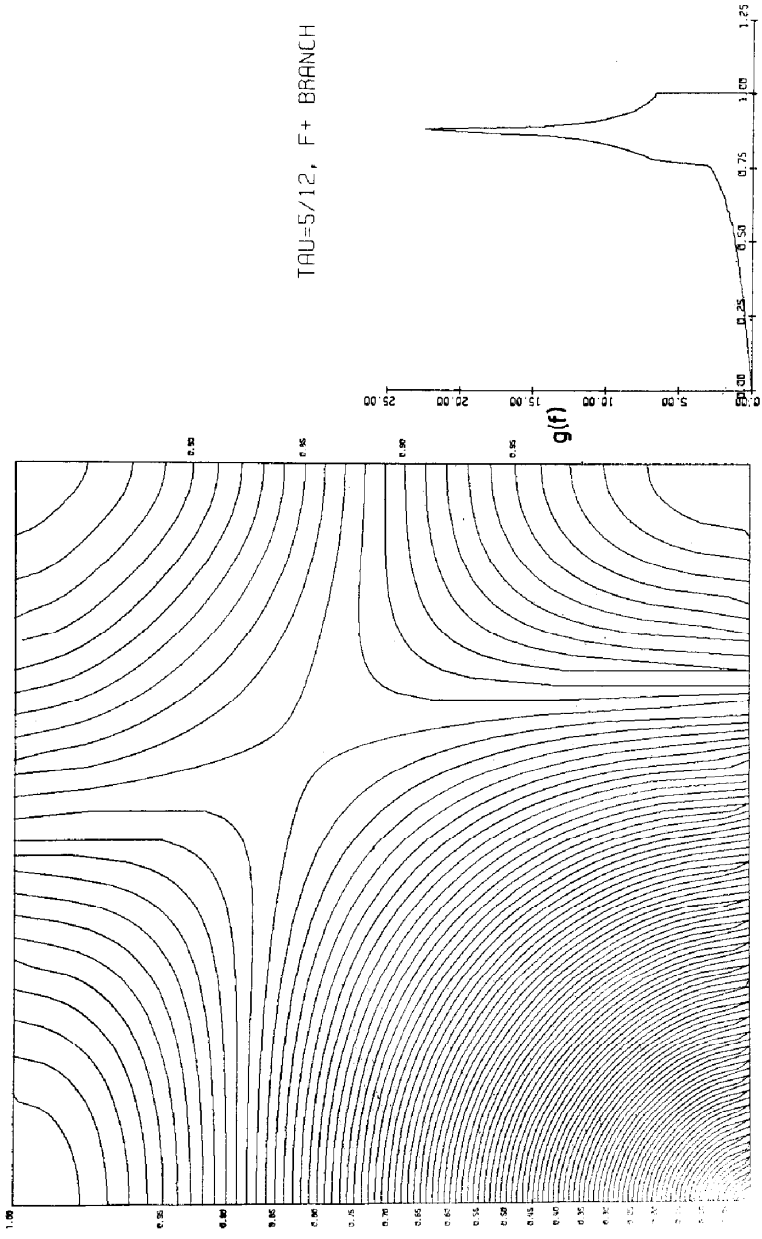

FIG. 5e. + branch, $\epsilon = 1$, and $\tau = \frac{5}{12}$.

Denoting the degree of anisotropy by the ratio $\alpha/\beta = \epsilon$ such that $0 \leqslant \epsilon \leqslant 1$, the largest frequency, ν_L, corresponding to the extremum of (9) is

$$\nu_L = [(4\beta + 8\gamma)/4\pi^2 M]^{1/2}. \tag{11}$$

By further defining

$$\tau = 8\gamma/4\pi^2 M\nu_L{}^2 = 1/[1 + (\beta/2\gamma)], \tag{12a}$$

$$c_j = \cos \phi_j, \tag{12b}$$

$$f = \nu/\nu_L, \tag{12c}$$

(9) expanded becomes a polynomial in c_2,

$$ac_2{}^2 + bc_2 + d = 0, \tag{13}$$

where

$$a = \tau^2 + \tau(1 - \tau)\, c_1, \tag{14a}$$

$$b = [1 - \tau][2f^2 - \tau - \epsilon(1 - \tau)] + c_1[4\tau f^2 - 2\tau^2 - (1 - \tau)(\tau + \epsilon(2\tau - 1))] + c_1{}^2\epsilon\tau(1 - \tau), \tag{14b}$$

$$d = 4f^2(f^2 - 1) - \epsilon(1 - \tau)(2f^2 - 1) + (1 - \tau)(\tau + 2f^2) + c_1\epsilon(1 - \tau)(2f^2 - 1) + c_1{}^2\tau^2. \tag{14c}$$

The determinant (9) is, of course, also a quadratic equation in ν^2 with real solutions for all relevant c_1 and c_2. Thus there are two distinct branches (shown in Fig. 1a, for τ near $\frac{1}{3}$ and ϵ near 1). It is therefore appropriate to compute their spectra separately. This complicates the routine somewhat, since the choice of "+" or "—" in the solution of (13) for c_2 corresponds in no simple way to the choice for ν^2 in (9), and a decision routine must be added.

Figures 1 and 4 show contour maps and vibrational spectra g for + and — frequency branches with various values of τ and ϵ. The case $\tau = \frac{1}{3}$, $\epsilon = 1$ corresponds to the case analytically solved by Montroll [7], and his analytic results are included for comparison (Figs. 5c, d).

The relation between the contours, the geometry of the surface they belong to, and the spectrum should be clarified by reference to Figs. 1a–c. In two dimensions a smooth local extremum (such as those at A, B, C) gives a jump discontinuity in g (though no jump in dg/df). The nondifferentiable minimum at 0 of each branch is tangential to a cone at 0, giving a linear increase from zero.

D, E, F, G, H are saddle singularities: recall that the surfaces extend to cover all ϕ-space by reflections in the planes $\phi_1 = n\pi$, $\phi_2 = n\pi$. As f approaches a local

extremum, the lengths of neighboring contours decrease as the flatness of the surface increases their separation. This accounts for the local contribution to g, the area between contours flattening toward a constant before vanishing. Toward a saddle, both increase, and g has a logarithmic singularity.

If two singularities are not separated by more than one or two contours (as D, E and G, H are not), a finer spacing of energy values may be needed to separate them clearly in the spectrum.

Note that Fig. 5a has a complicated saddle in the upper right corner. This is not a Morse singularity, but is stable with respect to variations that preserve the high degree of symmetry at that point. If ϵ becomes $\neq 1$, it bifurcates into two minima and five normal saddles (Figs. 1b, 5b); if τ increases past $\frac{1}{5}$ and ϵ remains 1, it bifurcates into one minimum and four normal saddles (Figs. 5c, e). These illustrate the fact that for index theorem purposes [21] it is equivalent to three normal saddles ($2 - 5 = 1 - 4 = -3$).

III. An Electronic Example

The electronic states of solids are theoretically treated by two zero-order approximations, one being the very localized Heitler–London method and the other being the extremely delocalized Bloch model. Molecular and ionic crystals have low-lying excited states and are therefore best described in terms of their component free molecules or ions. Metals and semiconductors lie on the other side of the spectrum, however, and have free-electron-like wavefunctions. During the past 35 years a molecular approach, the free electron orbital method (FEMO) has been developed to describe the electronic properties of matter in a simple way. In this model Π-electrons are restricted to move along the bonds of a planar conjugated system under the influence of a potential field which is, in first approximation, constant. Pauling [13] first used this description to explain the diamagnetism of aromatic molecules, Schmidt [14] generalized it further by thinking of the conjugated system as a large flat box, analogous to the 2-dimensional model of graphite, containing a Fermi gas of Π-electrons, while Della Riccia [15] employed it in computing the band structure of diamond. Ruedenberg and Scherr [16] and Platt [17] have also used this model in their discussions of the ultraviolet spectra for a variety of ring structure organic molecules and for hydrocarbon chains with conjugated double bonds. Recently a nework model of electrons in solids has been introduced by Montroll [2] in which the electrons are restricted by nonconstant potential fields to move along the bonds of a periodic network of atoms. The network is given the same topological pattern with the same lattice spacings that would represent its crystallographic characterization. The two basic features of FEMO are incorporated in this model, that is,

(i) the wavefunction is continuous along all branches of the network and at

It should be noted that the first condition only holds true for atoms with dimensions of measure zero, i.e., atoms represented as points. Condition (ii) has the flavor of a "Kirchhoff"-like current law. It can be shown that in the stationary state the momentum conservation condition (ii) has, for an arbitrary potential $V(x)$, the form

$$\sum_{\{\mathbf{j}_\rho\}} \psi'(\mathbf{j}_\rho)\Big|_{\mathbf{j}=\text{node}} = 0, \tag{15}$$

where the sum is taken over all nearest-neighbor points $\mathbf{j}_\rho$ to $\mathbf{j}$. The energy band structure is then obtained by invoking into (15) the appropriate periodic boundary conditions which correspond to the translational symmetry of the lattice. As an illustration, the band structure for a d-dimensional, $1 \leqslant d \leqslant 3$, S.C.C. lattice having bond length l is found from the form factor equation

$$2dF(k, \alpha)\ \psi(\mathbf{j}) = \sum_{\{\mathbf{j}_\rho\}} \psi(\mathbf{j}_\rho), \tag{16}$$

where the functional form of $F(k, \alpha)$ is potential dependent. For convenience we choose as our atomic potential

$$V(x) = -V_0 \operatorname{sech}^2 \gamma x, \tag{17a}$$

since this has the property that as the depth of the potential becomes large, one obtains a tight binding situation and as the potential vanishes and the number of node points increases, one obtains the Sommerfeld free electron model. γ may be thought of as a force constant and when expressing V_0 as

$$V_0 = r(r+1)(\hbar^2\gamma^2/2m), \tag{17b}$$

one finds that the wavefunctions, for positive integral values of r, are elementary functions. For example, when $r = 1$,

$$\psi(x) = a[\cos(kx + \delta) - (\gamma/k)\sin(kx + \delta)\tanh \gamma x], \tag{18}$$

a, δ being the constants of integration of the Schrödinger equation and where k is related to the energy levels by $k^2 = 2mE/\hbar^2$. $F(k, \alpha)$ is then

$$(c^2 - s^2 + cu - sv)/(1 + cu + sv), \tag{19}$$

where

$$\tan\theta(x) = (\gamma/k)\tanh\gamma x, \qquad \text{with} \quad -\pi < \theta(x) < \pi, \tag{20a}$$

$$\theta \equiv \theta(l/2), \tag{20b}$$

$$c = \cos[(kl/2) + \theta], \tag{20c}$$

$$s = \sin[(kl/2) + \theta], \tag{20d}$$

$$u = (\gamma/k)^2 \cos\theta \operatorname{sech}^2(\gamma l/2)\cos(kl/2), \tag{20e}$$

$$v = (\gamma/k)^2 \cos\theta \operatorname{sech}^2(\gamma l/2)\sin(kl/2), \tag{20f}$$

and

$$\alpha = \gamma l/2. \tag{20g}$$

For k real, Eq. (2) will determine the allowable conduction band states while for k imaginary it will determine the bound state band structure.

For the purpose of further discussion it will be advantageous to express the current condition (15) in terms of the wavefunction in (18). We consider the schematic representation of a bond of length l connecting nodes i and j,

$$\overline{i \qquad x \qquad j},$$

with the x denoting the midpoint of the bond. The wavefunction, $\psi(i)$, associated with the atom at i must connect at the x in a continuous manner with the wavefunction, $\psi(j)$, associated with the atom at j. Thus, since

$$\psi(0) = a\cos\delta, \tag{21a}$$

$$-\psi'(0)/\psi(0) = -k[1 + (\gamma/k)^2]\tan\delta, \tag{21b}$$

0 referring to some origin, i or j, one finds that at the midpoint $l/2$,

$$\psi(l/2) = \psi(i)\cos[\theta + (kl/2) + \delta_{ij}]/\cos\delta_{ij}, \tag{22a}$$

$$\psi(-l/2) = \psi(j)\cos[\theta + (kl/2) - \delta_{ji}]/\cos\delta_{ji}, \tag{22b}$$

δ_{mn} representing the phase factor going from m to n.

Equating these two we derive

$$\psi(i)[c - s\tan\delta_{ij}] - \psi(j)[c + s\tan\delta_{ji}] = 0. \tag{23}$$

In a similar manner, if we equate the two derivatives at x, we find

$$\psi(i)[(c + u)\tan\delta_{ij} + s + v] - \psi(j)[(c + u)\tan\delta_{ji} - s - v] = 0. \tag{24}$$

Eliminating the phase factor δ_{ji} from Eqs. (23) and (24) leads to the relationship for tan δ_{ij},

$$-\tan \delta_{ij} = \frac{\psi(j)}{\psi(i)} \frac{(1 + cu + sv)}{2s(c + u)} - \frac{(c^2 - s^2 + cu - sv)}{2s(c + u)}. \tag{25}$$

Summing (25) over all bonds connected to node i we see, from inspection of (21b), that the current conservation condition is

$$-\sum_{\rho} k(1 + (\gamma/k)^2) \tan \delta_{ij_\rho} = 0. \tag{26a}$$

In the limit as $\gamma \to 0$, i.e., the free electron case, (26a) becomes

$$-\sum_{\rho} k \tan \delta_{ij_\rho} = 0. \tag{26b}$$

In the following section we shall construct a network model of a 2-dimensional polyethylene crystal. From its dispersion relation we then calculate the density of states both analytically and with this histogram method.

IV. A Model "Polyethylene" Crystal

Due to its chemical simplicity all normally produced specimens of polyethylene are highly crystalline, having space group Pnam and containing four CH_2 monomers per unit cell. The unit cell dimensions for cold drawn threads and for rolled sheets are variable depending on the amount of methyl branching that occurs. The more branching within the crystallite the larger the spacing between molecular chains, which consequently results in unit cell expansion. Along the fiber axis the repeat distance c is the repeat distance along a planar zig-zag chain of singly bound carbon atoms with normal bond angles and bond lengths. The a and b dimensions characterize the side-by-side packing of the chains. Thus, the unit cell lattice parameters have values $c = 2.534$ Å, $a = 7.36$ Å–7.68 Å, and $b = 4.94$ Å–5.00 Å. The molecular packing in a unit cell is shown in Fig. 6 [18, 19, 20]. For this particular calculation we shall only be concerned with toroidal sheets of skeletal polyethylene molecules (hydrogen atoms are not included) arranged as in Fig. 7 [3]. For simplicity, the translational symmetry is presumed to be two-dimensional simple cubic. Thus, there are two carbon atoms per unit cell. The electrons are constrained to move only along the "bonds" of the system and in such a way that within a chain the atomic potential, $V(x)$, is set at zero and between chains as $V(x) = -(\gamma^2\hbar^2/m)\,\mathrm{sech}^2\,\gamma x$. The electron must therefore tunnel through a poten-

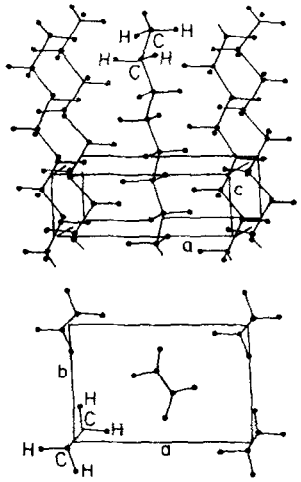

FIG. 6. Arrangement of molecules in polyethylene crystallites. From Meares [18].

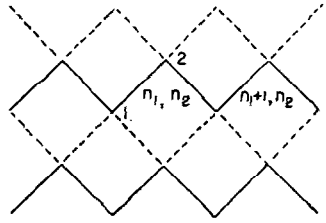

FIG. 7. Model of 2-D "Polyethylene." No potential exists along the solid bonds. A potential of the form $V(x) = -V_0 \operatorname{sech}^2 \gamma x$ exists along the dotted bonds.

tial barrier of half-width $\gamma^{-1} \tanh^{-1}(0.5)$ in order to traverse the interchain bond distance of l.

By utilizing the phase relations (26a) and (26b), the former along the polyethylene chain and the latter between chains, and the current conservation condition at the node points we obtain the set of coupled equations

$$\begin{aligned} &z_1\psi_1(n_1, n_2) - \psi_2(n_1, n_2) - \psi_2(n_1 - 1, n_2) \\ &\quad - \mu(\psi_2(n_1 - 1, n_2 - 1) + \psi_2(n_1, n_2 - 1)) = 0, \\ &z_1\psi_2(n_1, n_2) - \psi_1(n_1, n_2) - \psi_1(n_1 + 1, n_2) \\ &\quad - \mu(\psi_1(n_1 + 1, n_2 + 1) + \psi_1(n_1, n_2 + 1)) = 0, \end{aligned} \tag{27}$$

where $\psi_i(n_1, n_2)$, $i = 1, 2$, is the wavefunction of atoms 1 and 2 located at the unit

cell coordinates (n_1, n_2), and where z_1 and μ are energy functions, respectively defined as

$$z_1 = \sin kl[(1 + (\gamma/k)^2)((c^2 - s^2 + cu - sv)/2s(c + u)) + ctn\, kl], \quad (28a)$$

$$\mu = \sin kl(1 + (\gamma/k)^2)(1 + cu + sv)/2s(c + u). \quad (28b)$$

Employing the cyclic boundary conditions

$$\psi_i(n_1, n_2) = \psi_i(n_1 \pm N_1, n_2) = \psi_i(n_1, n_2 \pm N_2) = \psi_i(n_1 \pm N_1, n_2 \pm N_2), \quad (29)$$

where N_1, N_2 are the total number of unit cells in the n_1 and n_2 directions, respectively, one can represent ψ_1 and ψ_2 as

$$\psi_1 = A_1 \exp(n_1\phi_1 + n_2\phi_2), \quad (30a)$$

$$\psi_2 = A_2 \exp(n_1\phi_1 + n_2\phi_2), \quad (30b)$$

A_1, A_2 being normalization constants.

The solution to this set of coupled equations is found by setting the determinant of the coefficients of (27) to zero, i.e., det $M_{el} = 0$, and becomes

$$2z_1^2 = (1 + \cos\phi_1)(\mu^2 + 2\mu\cos\phi_2 + 1). \quad (31)$$

This equation determines the energy band structure of the system.

The density of states corresponding to the dispersion relation (31) can be found analytically from

$$D(E) = \left| \frac{\partial}{\partial E} N(E) \right|, \quad (32)$$

where $N(E)$ is the total integrated area between the curves of constant energy from E' and some maximum value E in $\phi_1 - \phi_2$ space (reduced Brillouin zone).

$$N(E) = \iint_{E'<E} \phi_1 \, d\phi_2 \quad (33)$$

Thus, from (31)

$$D(E) = \left| \frac{\partial}{\partial E} \int_{E'<E} \cos^{-1}\left(\frac{2z_1^2}{(\mu^2 + 2\mu\cos\phi_2 + 1)} - 1 \right) d\phi_2 \right| \quad (34a)$$

$$= \left| \frac{dk}{dE} \right| \left| \int \frac{(\mu^2+2\mu\cos\phi_2+1)(d/dk)\, 2z_1 - z_1(d/dk)(\mu^2+2\mu\cos\phi_2+1)\, d\phi_2}{(\mu^2 + 2\mu\cos\phi_2 + 1)[\mu^2 + 2\mu\cos\phi_2 + 1 - z_1^2]^{1/2}} \right|, \quad (34b)$$

where

$$\frac{dz_1}{dk} = \frac{dz_1}{dE}\frac{dE}{dk} = \frac{d}{dE}\left(\mu\frac{G}{H} + \cos kl\right)\frac{dE}{dk}. \tag{34c}$$

The derivative functions in E are given in the Appendix. Since ϕ_1 and ϕ_2 are both symmetric around 0 we need only restrict ourselves to an integration over one quadrant of the reduced Brillouin zone, that is, when $0 \leqslant \phi_1 \leqslant \pi$ and $0 \leqslant \phi_2 \leqslant \pi$. From closer inspection of the dispersion relation contribution to the integral in (34b) arises only when

$$-1 \leqslant [2z_1^2/(\mu^2 + 2\mu\cos\phi_2 + 1)] - 1 \leqslant 1. \tag{35}$$

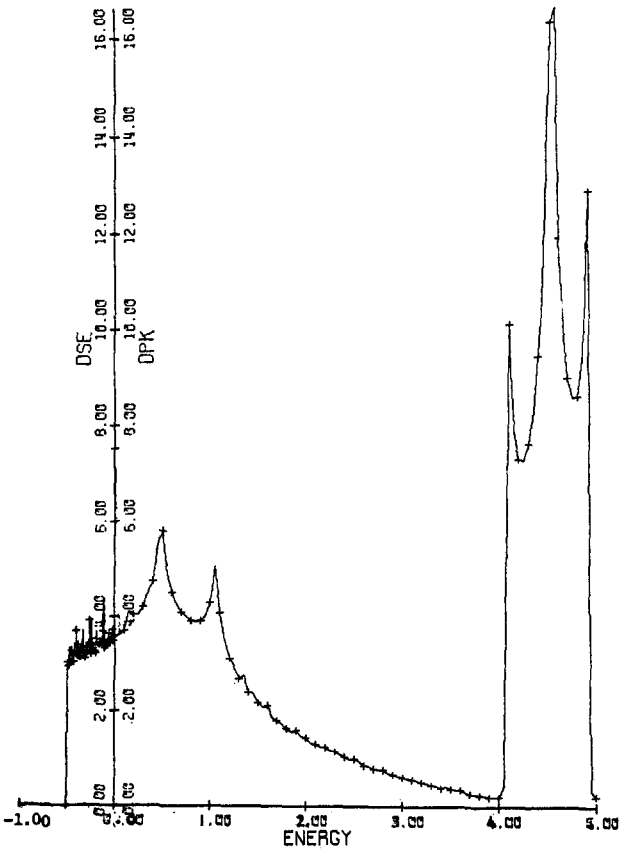

FIG. 8. Density of states for 2-D "Polyethylene" model obtained by analytically evaluating (34b) when $\alpha = \frac{1}{2}$. DPK stands for density of conduction band states and *DSE* stands for density of bound state band states. The very rough look to DSE is a result of a much finer E mesh than was used for DPK.

Figure 8 exhibits $D(E)$ when $\alpha = \gamma l/2 = \frac{1}{2}$. This spectrum incorporates the fact that due to the Pauli Exclusion Principle for Fermi particles $D(E)$ must be multiplied by a factor of 2.

The contour map in $\phi_1 - \phi_2$ space corresponding to the dispersion relation (31) is given in Fig. 9a. From the energy contours it is clear that due to energy splitting between the two atoms in the polyethylene unit we are dealing with two surfaces in each of two bands with the division in bands occurring between contours 93 and 94 and corresponds to the beginning of the first excited state band. The ground state energy band begins between energies -0.5 and -0.55. The four singularities correspond to saddles located between contours 22 and 23, 33 and 34, 102 and 103, and 103 and 104. Agreement with the analytical $D(E)$ result is excellent (Fig. 9b).

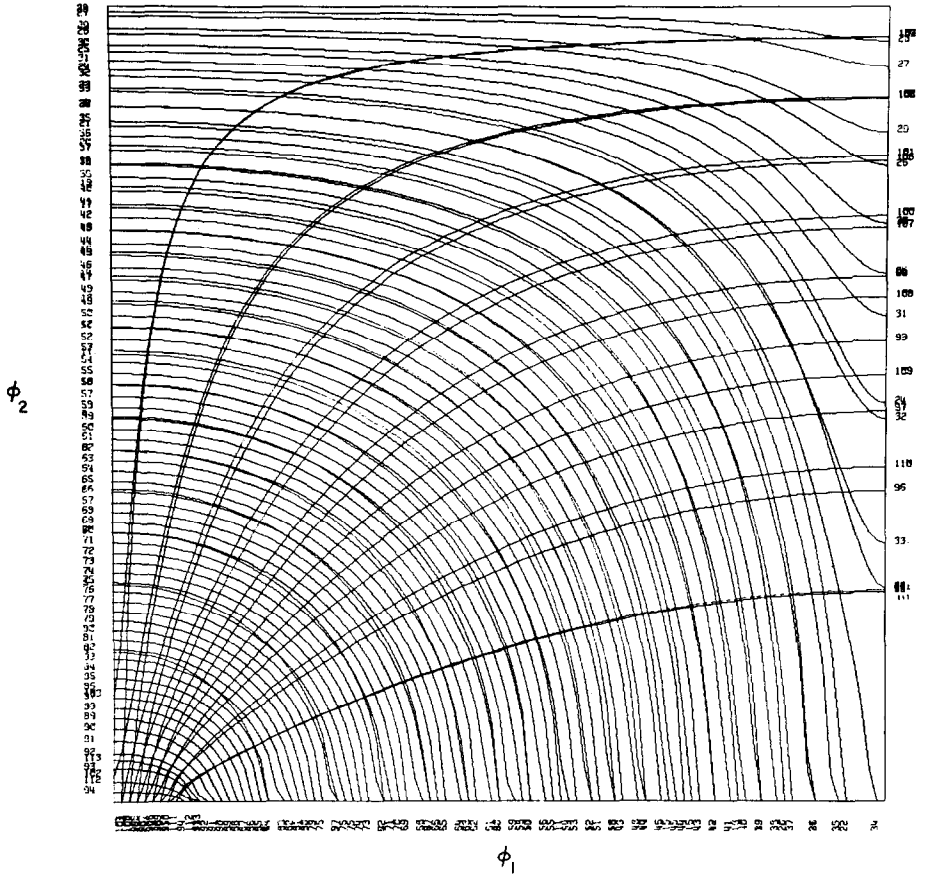

FIG. 9a. Contour map corresponding to the dispersion relation (31).

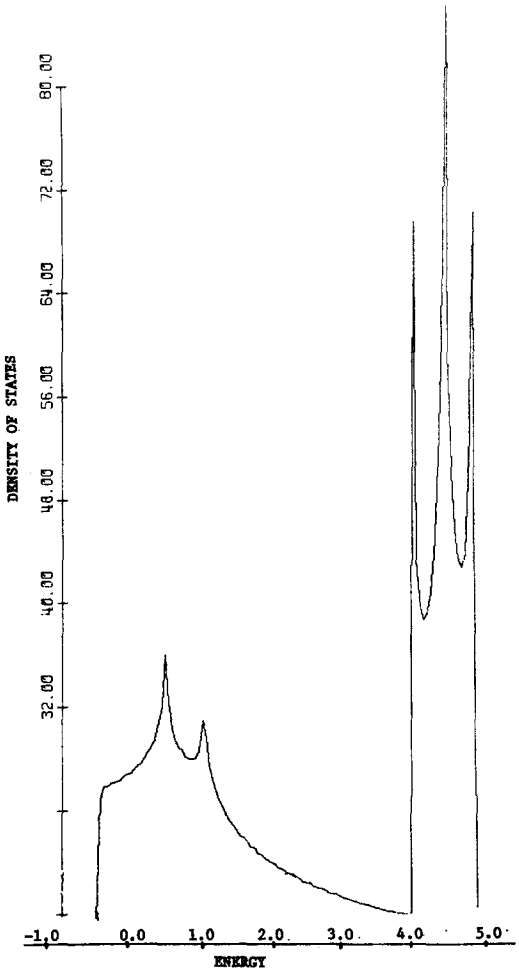

FIG. 9b. Density of states obtained from the energy contours in Fig. 9a.

V. COMPUTATIONAL DATA

In obtaining each of the spectra in Figs. 1b, 1c, and 5, for each of 101 values of f^2, $0 \leqslant f^2 \leqslant 1$, ϕ_1 was varied between 0 and π in 101 increments. The total computational time on an IBM 360-65 was approximately 43 sec.

For the electronic spectra in Figs. 8 and 9b the energy grid varied between -0.6 and 5.0. In doing the analytic computation (Fig. 9a) we subdivided the energy ranges $[-0.6, 0]$ and [0., 5.0] into 101 segments each. The integral in (34b)

was then evaluated by using Simpson's rule with a grid of 500 points distributed in $[0, \pi]$. The total computational time required was approximately 1 min and 55 sec. The geometric approach utilized 114 values of E in the above ranges, with 101 ϕ_2 values. The total computational time required was 19 sec.

Appendix

The derivative functions of z_1 in Eq. (28a), letting $K = k/\gamma$, are

$$\frac{d(G/H)}{dE} = 2[2K^2 \tanh \alpha - \alpha(1 + K^2)(2K^2 + \operatorname{sech}^2 \alpha)] \frac{\tanh \alpha \cos kl}{K^2(1 + K^2)^2} + \frac{\sin kl}{K^3(1 + K^2)^2} \{[2K^2(K^2 - 1) + (3K^2 + 1) \operatorname{sech}^2 \alpha] \tanh \alpha - 2\alpha K^2(1 + K^2)(K^2 + 1 - 2 \tanh^2 \alpha)\}, \tag{A.1}$$

$$\frac{dH}{dE} = \frac{2}{KQ} \cosh^2 \alpha(1 + K^{-2})[(K(1 + K^{-2}) - 2K^{-1}) \Delta - K^{-1} \tanh^2 \alpha(1 + K^{-2})] - \frac{2H}{KQ} \left[K \cosh^2 \alpha(\sin kl[\rho - \Delta] + 2K^{-1} \tanh \alpha \left(\rho \cos^2 \frac{kl}{2} - 1\right)\right] + (\cosh^2 \alpha(1 + K^2) - 1)(\alpha(\rho - \Delta) \cos kl + K^{-3} \sin kl(1 - 2 \operatorname{sech}^2 \alpha) - K^{-1} \tanh \alpha \left(K^{-1} \left(\rho \cos^2 \frac{kl}{2} - 1\right) + 2K^{-3} \cos^2 \frac{kl}{2} \operatorname{sech}^2 \alpha + \alpha\rho \sin kl\right)\right)\Big], \tag{A.2}$$

where

$$Q = [\cosh^2 \alpha(1 + K^2) - 1] \left[\sin kl(\rho - \Delta) + 2K^{-1} \tanh \alpha \left(\rho \cos^2 \frac{kl}{2} - 1\right)\right], \tag{A.3a}$$

$$\rho = 2 + K^{-2} \operatorname{sech}^2 \alpha, \tag{A.3b}$$

and

$$\Delta = 1 + K^{-2} \tanh^2 \alpha, \tag{A.3c}$$

and finally,

$$\frac{d\mu}{dE} = \frac{2\alpha}{K} \cos kl \cdot H + (\sin kl) \frac{dH}{dE}. \tag{A.4}$$

ACKNOWLEDGMENT

The authors thank Professor E. W. Montroll for providing the facilities with which this project has been done, and the NSF for partial financial support. We also thank the referee for bringing to our attention the work of Faulkner *et al.*

REFERENCES

1. A. A. MARADUDIN, E. W. MONTROLL, G. H. WEISS, AND I. P. IPATOVA, "Theory of Lattice Dynamics in the Harmonic Approximation, Solid State Physics," Supplement 3, p. 16, Academic Press, New York, 1971.
2. E. W. MONTROLL, *J. Math. Phys.* **11** (1970), 635.
3. A. B. BUDGOR, Ph.D. Thesis, University of Rochester, 1974.
4. L. VAN HOVE, *Phys. Rev.* **89** (1953), 1189.
5. E. W. MONTROLL, *Amer. Math. Monthly* **61** (1954), 46.
6. M. BORN AND T. VON KARMAN, *Phys. Z.* **13** (1912), 297.
7. E. W. MONTROLL, *J. Chem. Phys.* **15** (1947), 575.
8. G. GILAT AND G. DOLLING, *Phys. Letters* **8** (1964), 304.
9. G. GILAT AND L. J. RAUBENHEIMER, *Phys. Rev.* **144** (1966), 320.
10. A. E. R. WOODCOCK AND T. POSTON, "The Geometry of the Elementary Catastrophes," Lecture Notes in Mathematics, Springer–Verlag, Berlin/New York, to appear.
11. A. B. BUDGOR, T. POSTON, AND E. W. MONTROLL, work in progress.
12. J. M. ZIMAN, "Principles of the Theory of Solids," pp. 68–98, Cambridge University Press, London/New York, 1965.
13. L. PAULING, *J. Chem. Phys.* **4** (1936), 673.
14. O. SCHMIDT, *Z. Physik Chem.* **47B** (1940), 1.
15. G. DELLA RICCIA, in "International Conference on the Physics of Semiconductors, Exeter," p. 570, Institute of Physics and the Physical Society, London, 1962.
16. K. RUEDENBERG AND C. W. SCHERR, *J. Chem. Phys.* **21** (1953), 1565; **22** (1954), 151.
17. J. R. PLATT, "Free Electron Theory of Conjugated Molecules," Wiley, 1964.
18. P. MEARES, "Polymers, Structure and Bulk Properties," Van Nostrand, London, 1965.
19. E. A. COLE AND D. R. HOLMES, *J. Polymer Sci.* **46** (1960), 245.
20. C. W. BUNN, *Trans. Faraday Soc.* **35** (1939), 482.
21. J. MILNOR, "Morse Theory," Annals of Math Studies 51, Princeton University Press, Princeton, N.J., 1963.
22. J. S. FAULKNER, H. L. DAVIS, AND H. W. JOY, *Phys. Rev.* **161** (1967), 656; J. S. FAULKNER, *Phys. Rev.* **178** (1969), 914.
23. L. J. RAUBENHEIMER AND G. GILAT, *Phys. Rev.* **157** (1967), 586.
24. Z. KAM AND G. GILAT, *Phys. Rev.* **175** (1968), 1156.